SUPPLEMENTARY INFORMATION

Synthesis of ternary NiCo-MnO_2 nanocomposite and its application as a novel high energy supercapattery device

Kabir O. Oyedotun, Moshawe J. Madito, Damilola Y. Momodu, Abdulmajid A. Mirghni, Tshifhiwa M. Masikhwa and Ncholu Manyala*

Department of Physics, Institute of Applied Materials, SARCHI Chair in Carbon Technology and Materials, University of Pretoria, Pretoria 0028, South Africa.

*Corresponding author's email: ncholu.manyala@up.ac.za, Tel.: + (27)12 420 3549

EXPERIMENTAL

Preparation of Polyaniline (PANI)

0.2 M of aniline hydrochloride (C_6H_8ClN) (2.59 g aniline hydrochloride in 50 ml deionized water) was added to 0.25 M of ammonium peroxydisulfate ($(NH_4)_2S_2O_8$) (5.71 g ammonium peroxysulfate in 50 ml deionized water. The mixture was stirred for 10 minutes, and then left to stand overnight for polymerization. The supernatant was decanted away and the recovered precipitate was washed several times with deionized. The resulting sample was dried overnight in an electric oven at 60 °C under ambient condition.

Preparation of carbonized iron cations adsorbed onto PANI (C-FP)

0.2 g iron (III) nitrate nonahydrate, 0.0125 g of polyaniline (PANI) and 0.026 g each of carbon acetylene black (CB) and PVDF were completely dissolved in ethanol (50 mL, 99.9 %) whilst magnetically stirring for 5 minutes. The precursors' masses were carefully selected to ensure an approximate weight ratio of 80:10:10 for iron (III) nitrate salt and PANI, CB and PVDF respectively. After 5 minutes of stirring, the resulting mixture was sonicated for several hours until slurry. The recovered slurry was then coated onto cut-to-

size nickel foam (1 cm × 1 cm) which was transferred into a chemical vapour deposition (CVD) system under N_2 atmosphere at 850 °C for 2 h to obtain iron cations adsorbed onto the PANI film (C-FP) directly grown onto the nickel foam.

The loading mass of the prepared the negative electrode was estimated to be approximately 4.0 mg cm^{-2} for the active material. The electrochemical impedance spectroscopy (EIS) of the samples was conducted in an open-circuit potential and in a range of 10 mHz to 100 kHz frequency at 0.0V potential.

The columbic efficiency, C_E as well as the specific capacitance, C_s (Fg^{-1}) (calculated according to equation 5) over a potential, V (V), of the nickel foam-supported negative electrode was estimated using the following relations:

$$C_E = \frac{t_D}{t_c} \times 100\% \qquad \text{ES1}$$

where C_s (F g^{-1}), I (A), Δt (s), ΔV (V), m (g), t_c and t_D, and C_E (%) are the specific capacitance, discharge current, discharge time, discharge potential window, active material mass, the times for charging and discharging with the same current, as well as the columbic efficiency respectively.

The average crystallite size of the as-synthesized samples was determined by the X-ray line broadening method via the Scherrer equation [1,7]:

$$L = \frac{k\lambda}{\beta Cos\theta} \qquad \text{ES2}$$

Where λ is the wavelength of the radiation used, CoKα in this case, k is the Scherrer constant, β is the full width at half maximum (FWHM) intensity of the diffraction peak for which the size is to be determined, θ is the diffraction angle of the particular peak, and L is the crystallite size.

RESULTS

Morphological, structural and elemental analyses

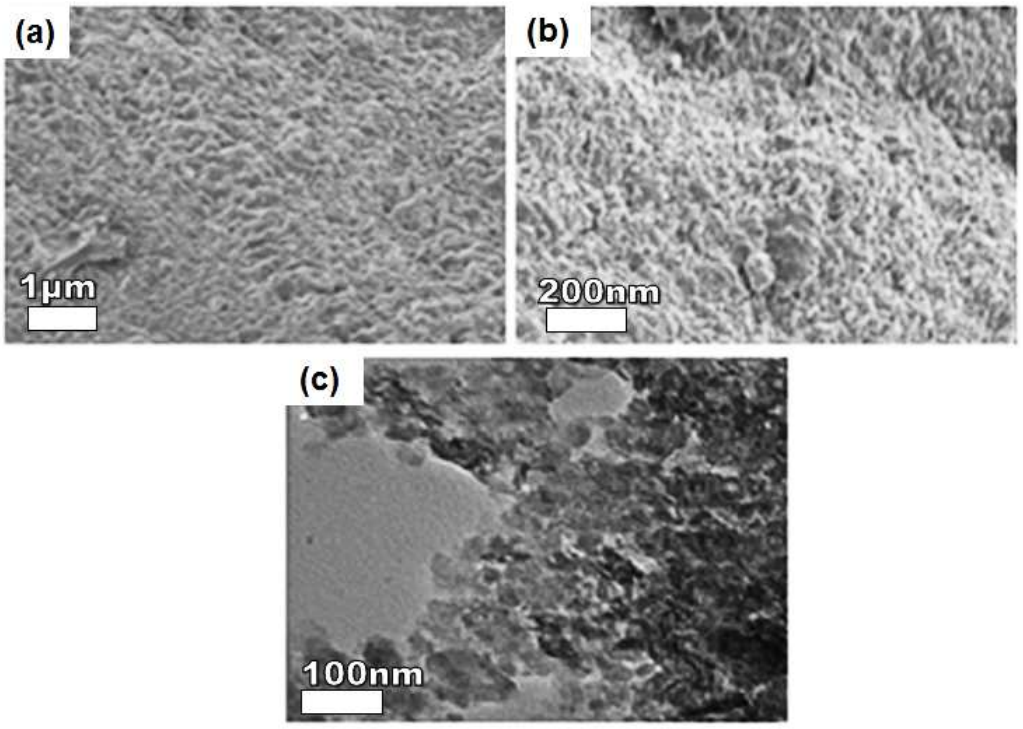

Fig. S1. (a) and (b) SEM images of the NiCoMn-TH at low and high magnifications respectively. (c) TEM image of the NiCoMn-TH.

Fig. S1 and S2 display the electron microscopy images at low and high magnifications of the NiCoMn-TH and as-synthesized C-FP electrodes respectively.

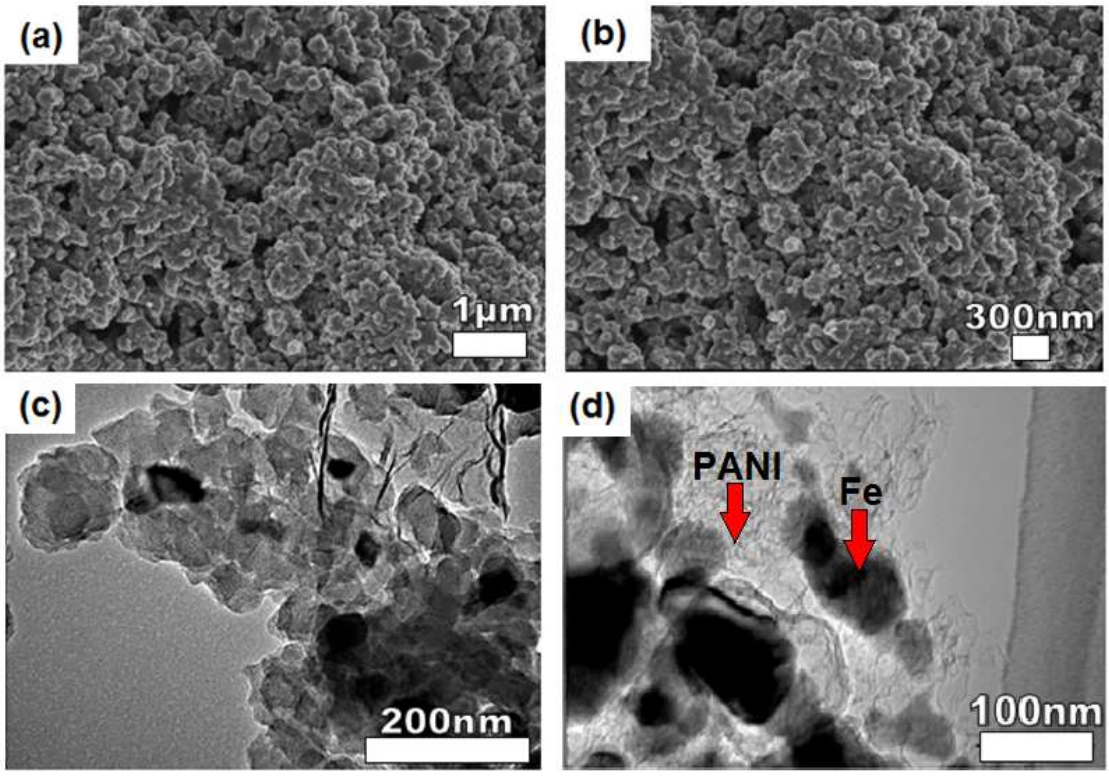

Fig. S2. (a) and (b) SEM images of the C-FP at low and high magnifications respectively. (c) and (d) TEM images of the C-FP at low and high magnifications respectively.

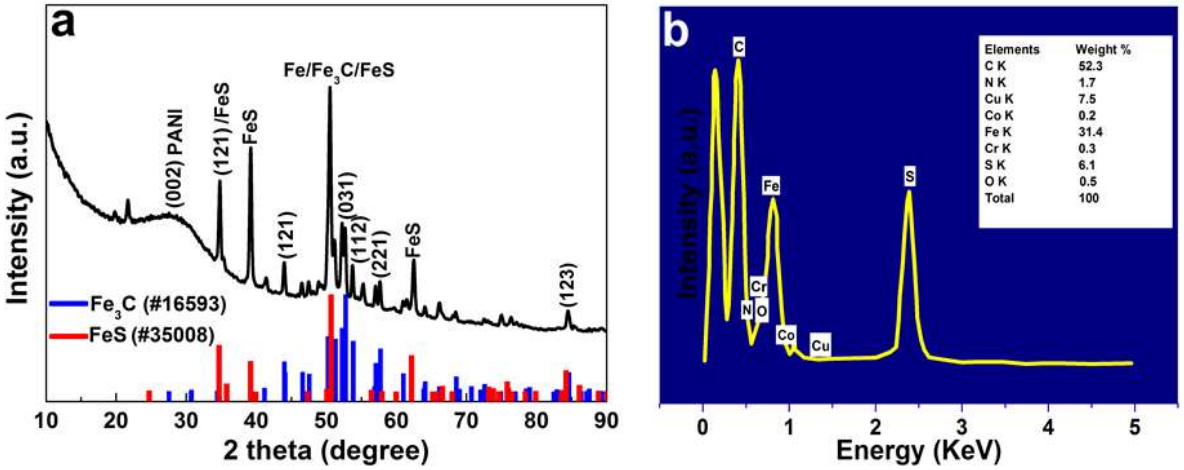

Fig. S3. (a) XRD spectrum and the matching ICSD card (b) EDX spectrum of the as-synthesized C-FP material respectively.

Fig. S3(a) shows the powder X-ray diffraction spectrum of the sample, and the best matching Inorganic Crystal Structure Database (ICSD) card no. 16593 with chemical formula Fe_3C (crystal system: orthorhombic and space-group: *Pnma*) and ICSD card no. 35008 with chemical formula FeS (crystal system: orthorhombic; space-group: *Pnma*) [2]. The XRD pattern shows a significant amount of orthorhombic Fe_3C predominantly due to the dissolution of carbon atoms into Fe lattices during pyrolysis at a high temperature of about 850 °C. In addition, the FeS diffraction peaks suggest that during the pyrolysis process the degradation of ammonium persulphate generated iron sulfide. The diffraction peak at about 52° could also be due to metallic Fe, in addition to Fe_3C and FeS diffraction. The XRD spectrum shows a broad peak for graphitic carbon; around 2θ = 30°, i.e. a (002) reflection [3]. Besides, the small size of the carbon nanoparticles could as well gives rise to peak broadening, an idea supported by the TEM micrographs results of the as-prepared C-FP sample (Fig. S2 (c-d)). The small peak at 2θ = 22.5 ° could be attributed to the presence of polyvinylidene fluoride (PVDF) used as the binder [4] .

The elemental analysis of the C-FP is as shown in Fig. S3 (b). The EDX spectra show that iron (31.4 wt. %) and carbon (52.3 wt. %) are the major elements present in the sample. The presence of sulphur (6.1 wt. %) and nitrogen (1.7 wt. %) in the EDX spectrum could be ascribed to the PANI composition. The elements Cu and other trace elements recorded in the spectra are portrayed owing to the grid sample holder for EDX analysis.

Electrochemical measurements of the C-FP

Fig. S4 displays the electrochemical performance of the C-FP electrode at different scan rates in a three-electrode configuration. The negative electrode material displayed no

noticeable peaks in its curves, S4 (a), with an ideal rectangular CV curves, showing the material's double-layer capacitive characteristics with good reversibility.

Fig. S4 (b) shows the CD profiles of the as-synthesized C-FP negative electrode at various current densities. The C-FP electrode specific capacitance is shown as function of current density in Fig. S4 (d). The cycling stability of C-FP was measured up to 1000 cycles at a charging–discharging current density of 5 A g^{-1} (S4 (e)). A coulombic efficiency of 102.6 % is observed for the electrode over 1000 cycling. The uniquely good cycling performance with relatively high specific capacitance is responsible for the material's good electrochemical performance. Fig. S4(c) displays Nyquist plot of C-FP electrode. The plot is observed to be composed of a nearly vertical line (Warburg line) within the low frequency region and a semicircle within the high frequency region indicating a typical capacitive behavior of EDLCs electrode [5,6].

Fig. S4 (f) shows the self-discharge (SD) curve of the hybrid NiCo-MnO_2//C-FP symmetric *SC* carried out at room temperature. From S4 (f), the *SC* was observed to maintain a substantial voltage of 1.11 V which indicates a good practical application of the hybrid *SC*.

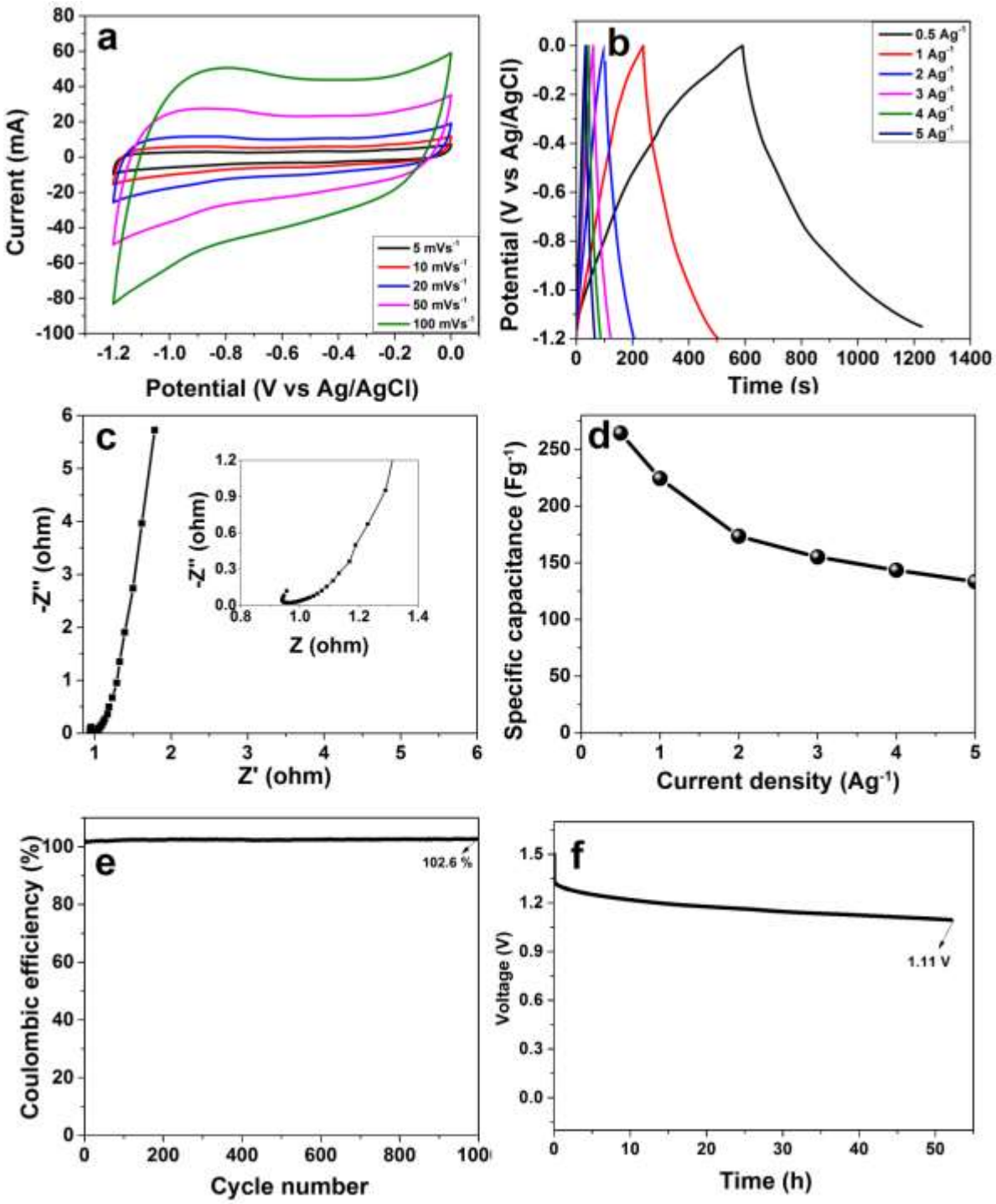

Fig. S4. (a) CV curves at various scan rates (b) CD profiles at various current densities (c) EIS Nyquist plot (d) Plot showing specific capacitance values against the current densities (e) plot showing efficiency against the cycle number for the as-prepared C-FP material respectively. (f) Self-discharge curve of the hybrid NiCo-MnO_2//C-FP asymmetric *SC*.

Table S1: Calculated values of R_s, R_{CT}, and Qs fitted parameters through ZFIT fitting of the experimental impedance spectra based on equivalent circuit shown in the inset to figure 13b.

Electrode	R_s (Ω)	R_{CT} (Ω)	Q_1 (F.s $^{(a-1)}$)	Q_2 (F.s $^{(a-1)}$)
NiCo-MnO_2//Fe_3C	0.22	1.94	0.03201	0.3274

Where R_s is the solution resistance, R_{CT} is the charge-transfer resistance, and Qs are the constant phase elements respectively.

Table S2: XRF data analysis of NiCo-MnO_2 as-prepared electrode material prepared as pressed powder.

Compounds	Weight %
Co	34.52
Mn	30.70
Ni	29.27
Cl	4.06
Na_2O	1.01
MgO	0.25
Eu_2O_3	0.08
SiO2	0.03
Tm_2O_3	0.03
MoO_3	0.02
CuO	0.02
Total	99.99

Loss on ignition = 0.01 Weight %.

REFERENCES

[1] S. Patra, P. Mitra, S.K. Pradhan, Preparation of nanodimensional CdS by chemical dipping technique and their characterization, Mater. Res. 14 (2011) 17–20. doi:10.1590/S1516-14392011005000015.

[2] R.T. Downs, M. Hall-Wallace, The American Mineralogist crystal structure database, Am. Mineral. 88 (2003) 247–250.

[3] K. W. Andrews, The structure of cementite, Acta Metall. 11 (1963) 939–946.

[4] J.P. Cheng, L. Liu, J. Zhang, F. Liu, X.B. Zhang, Influences of anion exchange and phase transformation on the supercapacitive properties of α-Co(OH)2, J. Electroanal. Chem. 722–723 (2014) 23–31. doi:10.1016/j.jelechem.2014.03.019.

[5] M. Yan, Y. Yao, J. Wen, W. Fu, L. Long, M. Wang, X. Liao, G. Yin, Z. Huang, X. Chen, A facile method to synthesize Fe<inf>x</inf>C<inf>y</inf>/C composite as negative electrode with high capacitance for supercapacitor, J. Alloys Compd. 641 (2015) 170–175. doi:10.1016/j.jallcom.2015.04.024.

[6] Y. Wang, G. Zhang, G. Liu, W. Liu, H. Chen, J. Yang, Facile synthesis of highly porous N-doped CNTs/Fe $_3$ C and its electrochemical properties, RSC Adv. 6 (2016) 44013–44018. doi:10.1039/C6RA07101E.

[7] H. P. Klug, & L. E. Alexander, X-Ray Diffraction Procedures: For Polycrystalline and Amorphous Materials, Wiley-VCH, May (1974) 992, ISBN 0-471-49369-4.